Rock and Soil Mechanics

Volume 44 | Issue 11 Article 3

2-2-2024

Study on the identification method of tunnel surrounding rock failure zone based on continuous discontinuous analysis theory

Ming-qing XIAO
China Railway Siyuan Survey and Design Group Co., Ltd., Wuhan, Hubei 430063, China; National & Local Joint Engineering Research Center of Underwater Tunneling Technology, Wuhan, Hubei 430063, China, tsyxmq@163.com

Chen XU
China Railway Siyuan Survey and Design Group Co., Ltd., Wuhan, Hubei 430063, China; National & Local Joint Engineering Research Center of Underwater Tunneling Technology, Wuhan, Hubei 430063, China

Jian YANG
China Railway Siyuan Survey and Design Group Co., Ltd., Wuhan, Hubei 430063, China; National & Local Joint Engineering Research Center of Underwater Tunneling Technology, Wuhan, Hubei 430063, China

Jia-ming WU
China Railway Siyuan Survey and Design Group Co., Ltd., Wuhan, Hubei 430063, China; National & Local Joint Engineering Research Center of Underwater Tunneling Technology, Wuhan, Hubei 430063, China

See next page for additional authors

Recommended Citation

XIAO, Ming-qing; XU, Chen; YANG, Jian; WU, Jia-ming; FU, Xiao-dong; and ZHOU, Yong-qiang (2024) "Study on the identification method of tunnel surrounding rock failure zone based on continuous discontinuous analysis theory," *Rock and Soil Mechanics*: Vol. 44: Iss. 11, Article 3.
DOI: 10.16285/j.rsm.2023.5652
Available at: https://rocksoilmech.researchcommons.org/journal/vol44/iss11/3

Study on the identification method of tunnel surrounding rock failure zone based on continuous discontinuous analysis theory

Abstract

Accurate analyzing the scope of tunnel excavation failure zone has important guidance and engineering significance in determining support parameters reasonably. This study focuses on the identification methods of tunnel surrounding rock failure zone, specifically the continuous medium analysis method and the continuous-discontinuous method represented by the finite element-discrete element coupling method (FDEM). Firstly, the continuous medium analysis method and FDEM identification criteria for surrounding rock failure are studied. Then the rock mass is divided into elastic rock elements and elastic-plastic interface elements. Based on the concept of equivalent continuous model, the relationship between the mechanical parameters of interface elements and rock elements and rock mass element is mathematically derived. The connection between the parameter values of these two methods is established for the first time, resolving the challenge of determining values in the continuous-discontinuous method. Finally, the ranges of surrounding rock failure zones simulated by these two methods during the excavation process of railway tunnels with different lithology and cross-sections are compared. According to the range of mechanical parameters for each class of surrounding rock mass in the specification, the range of values for the main failure parameters of surrounding rock, such as penalty parameter and fracture energy, in FDEM, is given for each class of surrounding rock. The simulation results of railway tunnel excavation with different lithology and cross sections using the continuous medium method represented by FLAC3D and FDEM method show that the plastic zone obtained by the continuous medium method, and the failure zone obtained by the plastic limit strain, as well as the crack growth zone and failure zone obtained by the continuous-discontinuous method, are generally consistent in terms of distribution range, shape and failure mode. The method proposed in this article for determining the failure parameters of surrounding rock in FDEM is verified as reasonable and feasible.

Keywords

continuous-discontinuous method, FDEM, tunnel, identification of failure zone, parameter values, continuous medium analysis method

Authors

Ming-qing XIAO, Chen XU, Jian YANG, Jia-ming WU, Xiao-dong FU, and Yong-qiang ZHOU

Rock and Soil Mechanics 2023 44(11): 3099−3108 ISSN 1000−7598
https://doi.org/10.16285/j.rsm.2023.5652 https://rocksoilmech.researchcommons.org/journal/

Study on the identification method of tunnel surrounding rock failure zone based on continuous discontinuous analysis theory

XIAO Ming-qing[1, 2], XU Chen[1, 2], YANG Jian[1, 2], WU Jia-ming[1, 2], FU Xiao-dong[3], ZHOU Yong-qiang[3]

1. China Railway Siyuan Survey and Design Group Co., Ltd., Wuhan, Hubei 430063, China

2. National & Local Joint Engineering Research Center of Underwater Tunneling Technology, Wuhan, Hubei 430063, China

3. State Key Laboratory of Geomechanics and Geotechnical Engineering, Institute of Rock and Soil Mechanics, Chinese Academy of Sciences, Wuhan, Hubei 430071, China

Abstract: Accurate analyzing the scope of tunnel excavation failure zone has important guidance and engineering significance in determining support parameters reasonably. This study focuses on the identification methods of tunnel surrounding rock failure zone, specifically the continuous medium analysis method and the continuous-discontinuous method represented by the finite element-discrete element coupling method (FDEM). Firstly, the continuous medium analysis method and FDEM identification criteria for surrounding rock failure are studied. Then the rock mass is divided into elastic rock elements and elastic-plastic interface elements. Based on the concept of equivalent continuous model, the relationship between the mechanical parameters of interface elements and rock elements and rock mass element is mathematically derived. The connection between the parameter values of these two methods is established for the first time, resolving the challenge of determining values in the continuous-discontinuous method. Finally, the ranges of surrounding rock failure zones simulated by these two methods during the excavation process of railway tunnels with different lithology and cross-sections are compared. According to the range of mechanical parameters for each class of surrounding rock mass in the specification, the range of values for the main failure parameters of surrounding rock, such as penalty parameter and fracture energy, in FDEM, is given for each class of surrounding rock. The simulation results of railway tunnel excavation with different lithology and cross sections using the continuous medium method represented by FLAC^{3D} and FDEM method show that the plastic zone obtained by the continuous medium method, and the failure zone obtained by the plastic limit strain, as well as the crack growth zone and failure zone obtained by the continuous-discontinuous method, are generally consistent in terms of distribution range, shape and failure mode. The method proposed in this article for determining the failure parameters of surrounding rock in FDEM is verified as reasonable and feasible.

Keywords: continuous-discontinuous method; FDEM; tunnel; identification of failure zone; parameter values; continuous medium analysis method

1 Introduction

With the vigorous development of Belt and Road Initiative in China, numerous strategic and lifeline projects, including the construction of tunnels, will be undertaken in the regions involved. Examples of these projects include the Dianzhong Water Diversion project and the West Route of the South-to-North Water Diversion project. Tunnels play a crucial role as a key component in major infrastructure projects, ensuring the security of resources for our country and friendly nations, and promoting social and economic development. They are an essential part of national construction and lifeline projects, and are also of paramount importance in terms of safe operation. Unloading induced by excavation causes stress redistribution in surrounding rock masses around the tunnel. Based on the extent of disturbance, the area near the excavation face can be divided into the in-situ stress zone, the soil-arch bearing zone (or plastic zone), and the loose failure zone[1]. The range and depth of the excavation failure zone play an important guiding role in determining the appropriate support parameters[2]. Plus, the condition of the working face is also determined by the range of the loose failure zone and whether effective and timely support measures are taken. Therefore, accurate analysis of the range of the excavation failure zone is of great engineering significance.

Regarding the failure zone of tunnel surrounding rocks, various theoretical formulas have been put forward, such as the natural collapsed arch theory [3] (for shallow-buried tunnels), the maximum horizontal stress theory[4] (for deep-buried tunnels), the surrounding rock loosened zone theory[5] (for deep-buried tunnels), and Fenner formula and Kastner formula[6–7] (for deep-buried tunnels). However, most of these theories are qualitative descriptions, making it difficult to quantitatively analyze the extent of the failure zone of surrounding rock masses. Fenner formula and Kastner formula can usually solely calculate the range of the failure zone under hydrostatic pressure. Numerical simulation methods have undergone significant advancements, with those based on the continuum medium being relatively straightforward and not

Received: 24 May 2023 Accepted: 10 September 2023
This work was supported by the National Key Research and Development Program (2021YFB2600400).
First author: XIAO Ming-qing, male, born in 1971, PhD, Professorate Senior Engineer, mainly engaged in the design and research of tunnels and underground engineering. E-mail:tsyxmq@163.com
Corresponding author: ZHOU Yong-qiang, male, born in 1990, PhD, Associate Professor, mainly engaged in research on geotechnical mechanics and engineering stability. E-mail: yqzhou@whrsm.ac.cn

demanding high-performance computing equipment. As a result, they have become the primary approach for analyzing the excavation failure zone of surrounding rock masses. For example, the excavation failure zone of tunnels has been numerically simulated using COMSOL by Huang et al.[8] and Hu at al.[9], using FLAC by Wu et al. [10], Chen et al. [11], Liu et al. [12] and Yuan et al. [13], using Phase2 by Li et al. [14], and using ABAQUS by Lei et al[15]. These software programs are based on the continuum medium theory and adopt ideal elastoplastic constitutive models for rocks. Therefore, the results of the failure zone in surrounding rock masses only indicate that the stress of surrounding rock masses exceeds its yield strength, but it does not necessarily mean that the surrounding rock masses are fractured, as they can still bear the load even in a plastic state[16]. To more accurately describe the post-peak softening state of rocks, the strain softening model [17], the elastoplastic damage model [18], and the elastoplastic brittle model[19] have been successively introduced into the analysis of the excavation failure zone of surrounding rock masses, achieving good results. However, Ma et al.[20] found that although the results using these methods is comparable with the field observation of brittle failure of tunnel surrounding rocks, the resultant range of the failure zone is larger. This attribute to a fact that the surrounding rocks maintain its continuity even after failure, which is conducive to the stress transfer between rock blocks and the development of the damage zone. In response to this, the continuous-discontinuous method, which can capture the entire progress of crack initiation, propagation, and coalescence, and better simulate the rock failure, has been applied. It combines the advantages of both continuous and discontinuous methods, where the initial state of the medium is considered as a continuum, and it can be transformed into a discontinuous medium based on the stress state during loading. Li et al.[21] used an improved PFC-FLAC discrete-continuous coupling method to study the microscopic mechanism and failure characteristics of local rock damage caused by underground chamber excavation. Ma et al.[20] compared the brittle failure characteristics of circular tunnel surrounding rocks using continuous and continuous-discontinuous methods, and found that the results obtained by continuous-discontinuous methods are closer to the field observation. Deng et al.[22–23] adopted the finite element-discrete element coupling method (FDEM) to simulate the fracturing and expansion process of deep tunnels, revealing the degree of rock fragmentation and the range of crack propagation. However, this method also has its limitations, such as the difficulty in determining model parameters. Although extensive research on parameter values for the continuous-discontinuous method has been conducted, suggested or trial values are usually offered, without reasonable theoretical formulas[24–25].

In addressing the aforementioned issues, this paper examines two methods: the continuous medium method and the continuous-discontinuous method represented by FDEM. Based on the basic theories and constitutive models of these two methods, the paper focuses on the criteria for identifying rock mass failure, and for the first time, establishes a theoretical connection between the parameter values of these two methods, thus solving the problem of parameter determination in the continuous-discontinuous method. Firstly, the criteria for identifying rock mass failure using the continuous medium method and FDEM were investigated. Secondly, rock masses were divided into elastic rock elements and elastoplastic interface elements. Based on the concept of an equivalent continuous model, the relationships between the mechanical parameters of the interface elements and the mechanical parameters of the rock elements as well as the rock mass elements were derived, thereby establishing the mathematic relationship between the mechanical parameters of rock as well as rock masses and the algorithm parameters of surrounding rock failure. Finally, the differences between the two methods, in simulating the range and failure pattern of the failure zone of surrounding rocks during the excavation of railway tunnels with different lithology and cross-sections, were compared.

2 Criteria for identifying rock mass failure using the continuous medium method and FDEM

2.1 Continuous medium method

From experimental results, rock materials generally go through elastic, peak, post-peak and residual stages, prior to final failure. To describe the mechanical properties of rock materials, classical ideal elastoplastic constitutive models were developed, such as the Mohr-Coulomb yield criterion, which can identify the transition from elasticity to plasticity, but cannot determine the state from plasticity to failure. To modify this type of model, Abell et al.[26] introduced the concept of ultimate strain. As shown in Fig. 1, the stress and strain of the rock element is denoted as σ and ε, respectively. The strains at which the rock element enters the plastic and failure state are denoted as the elastic and plastic ultimate strain, ε_{y} and ε_{f}, respectively. ε_{f} can be obtained as follows:

$$\varepsilon_{\mathrm{f}}=\frac{\varepsilon_1-\varepsilon_2}{\sqrt{3}} \tag{1}$$

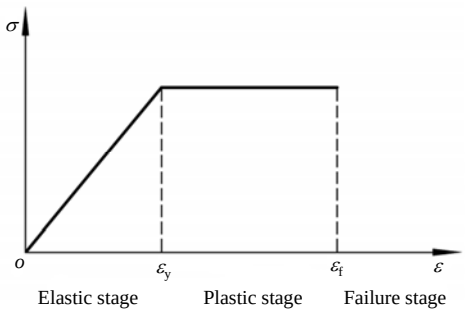

Fig. 1 Ideal elastoplastic constitutive model

where ε_1 and ε_2 represent the first and second principal strains, respectively. If strain exceeds ε_f, the rock element has undergone failure.

2.2 FDEM

FDEM is a method that combines the continuum method and the discontinuum method to study the process of rock failure and crack propagation. This method discretizes the simulation region into triangular finite elements, and inserts four-node joint elements with adhesive properties along the boundaries of finite elements. The transformation of the material from a continuous state to a discontinuous state is achieved through the softening and failure of the joint elements (Fig. 2).

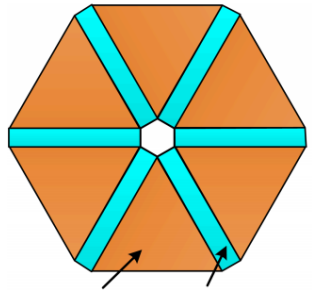

Fig. 2 Grid division principle in FDEM

Regarding the changes in mechanical properties near the crack tip, FDEM employs a cohesive fracture model that divides the stress–strain curve prior to macroscopic crack initiation into two parts, as shown in Fig.3, where f_t, f_s and f_r represent the tensile strength, shear strength, and residual shear strength of the joint element, respectively, and φ_i and φ_r denote the internal friction angle and residual internal friction angle of the joint element, respectively.

（1）Before the peak deformation——strain hardening stage

$$\sigma = \frac{p_{fn}}{h} \cdot o, \quad o < o_p \tag{2}$$

$$\tau = \frac{p_{fs}}{h} \cdot s, \quad s < s_p \tag{3}$$

where τ is the shear stress on the joint element; p_{fn} and p_{fs} represent the normal and tangential penalty parameter of the joint element, respectively; o and s represent the normal opening displacement and shear sliding displacement of the joint element, respectively; and o_p and s_p denote the displacement of the normal and tangential displacement of the joint element at the yield point, respectively; and h represents the size of the FDEM grid.

（2）After the peak deformation——strain softening stage

$$G_I = \int_{o_p}^{o_r} \sigma(o)\mathrm{d}o, \; o_p < o < o_r \tag{4}$$

$$G_{II} = \int_{s_p}^{s_r} \tau(s)\mathrm{d}s, \; s_p < s < s_r \tag{5}$$

where G_I and G_{II} represent the tensile and shear fracture energy of the joint element, respectively. o_r and s_r denote the normal and tangential displacement of the joint element at the failure point, respectively.

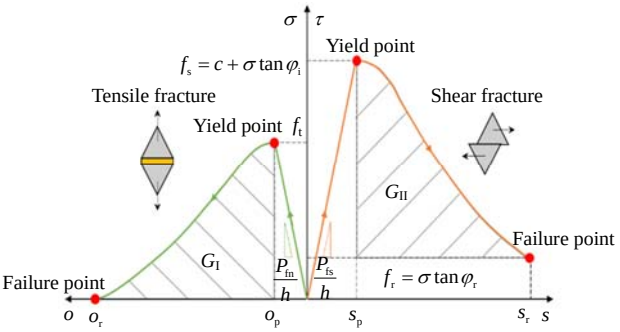

Fig. 3 Stress–strain relationship of joint elements in FDEM

The joint element will break once its strain reaches the limit. As an illustrative example, the tensile failure is shown in Fig.4. The opening displacement of the joint element is in the elastic stage before the critical value o_p; the damage representing microcracks begins to appear when the opening displacement reaches the critical value, and the material enters the softening stage; and at this point, the strength of microcracks does not abruptly decrease to zero, but rather gradually diminishes as the displacement increases. It continues to decrease until the opening displacement reaches the ultimate limit, at which point the strength is reduced to zero. This leads to the failure of the joint element and the emergence of macrocracks.

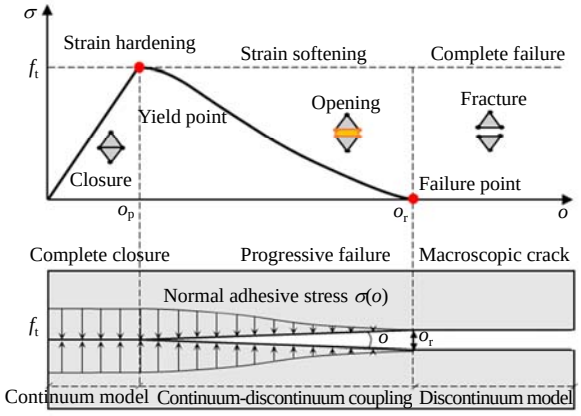

Fig. 4 Initiation and opening of joint elements in FDEM

3 Determining parameters of FDEM

The calculation in FDEM requires many micro parameters. According to the methods of obtaining these parameters, they can be divided into three categories [27]. The first category includes physical and mechanical properties of rocks, such as density ρ, elastic modulus E, Poisson's ratio μ, cohesion c, internal friction angle φ, and tensile strength T_s. The second category includes normal p_n and tangential

p_s penalty parameters for triangular solid elements, respectively, as well as normal p_{fn} and tangential p_{fs} penalty parameters for quadrilateral joint elements, respectively. The third category is fracture energy release rate G_I and G_{II} for tensile and shear failure of joint elements, respectively. The first category of mechanical parameters can be obtained through basic rock mechanics tests, such as uniaxial compression and Brazilian splitting tests. For the second category of penalty parameters, those for triangular elements, p_n and p_s, can reflect the deformation characteristics of intact rock blocks prior to yielding. Hence, their values can be equal to the elastic modulus E of intact rock blocks [28]. However, the penalty parameters for joint elements and the fracture energy parameters in the third category cannot be obtained through rock tests. In the current research on FDEM parameter calibration, Deng et al.[23] obtained the penalty parameters for joint elements and fracture energy through numerical simulation and calibration of uniaxial and Brazilian splitting tests. However, they did not provide a theoretical basis for determining those values. It has been demonstrated that the failure of tunnel rock masses is mainly shear [29]. This study hence focuses on the shear failure of joint elements in FDEM, and derives the relationships between the penalty parameters p_{fn} and p_{fs} of joint elements as well as shear fracture energy G_{II} and mechanical parameters of rock and rock mass elements.

3.1 Theory of homogenization

The theory of homogenization treats the structural planes in geomaterials as weak interlayers with a certain thickness, and rock mass elements are divided into rock elements and joint elements, as shown in Fig. 5. To simplify calculation, this study only considers two-dimensional plane stress conditions. The stress $\boldsymbol{\sigma}$ and strain $\boldsymbol{\varepsilon}$ components of elements include $\{\sigma_x,\sigma_y,\tau_{xy}\}^{\mathrm{T}}$ and $\{\varepsilon_x,\varepsilon_y,\gamma_{xy}\}^{\mathrm{T}}$, respectively. The relative displacement between the joints and the rock occurs within the joint units, while the two interfaces remain fully bonded. In the vicinity of the joints, according to the volumetric proportion between the joints and the rock, the stress and strain increments of the equivalent rock mass element satisfy the Eqs. (6) and (7):

$$\mathrm{d}\boldsymbol{\sigma}^{\mathrm{m}} = n^{\mathrm{r}}\mathrm{d}\boldsymbol{\sigma}^{\mathrm{r}} + n^{\mathrm{j}}\mathrm{d}\boldsymbol{\sigma}^{\mathrm{j}} \tag{6}$$

$$\mathrm{d}\boldsymbol{\varepsilon}^{\mathrm{m}} = n^{\mathrm{r}}\mathrm{d}\boldsymbol{\varepsilon}^{\mathrm{r}} + n^{\mathrm{j}}\mathrm{d}\boldsymbol{\varepsilon}^{\mathrm{j}} \tag{7}$$

where superscripts m, r, and j represent the rock mass element, rock element, and joint element, respectively. Parameters n^{r} and n^{j} represent the volume percentage of the rock element and joint element, respectively. If the assumed equivalent area has two parallel surfaces to the joint, the values of n^{r} and n^{j} are determined using the equations $n^{\mathrm{r}} = 1 - t/h$ and $n^{\mathrm{j}} = t/h$, respectively, where t is the thickness of the joint element and h is the overall thickness of the equivalent area.

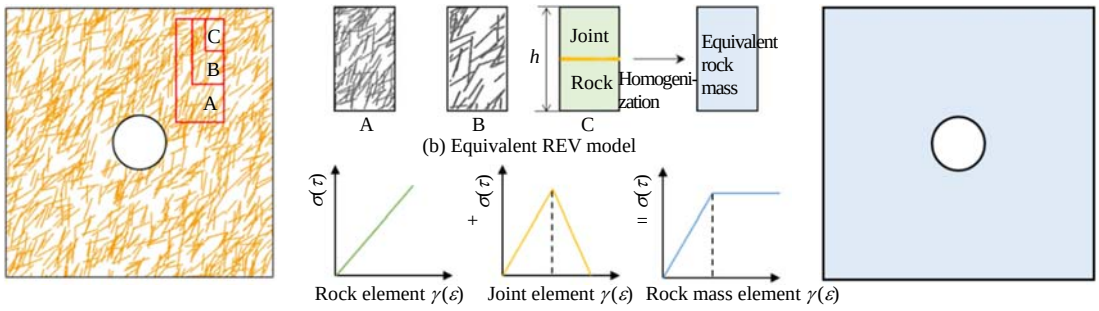

(a) A cavity in rock masses with numeroius joints (c) Constitutive relationship of equivalent rock mass (d) An equivalent cavity in rock masses

Fig. 5 Schematic diagram of homogenized equivalent rock masses

3.2 Deduction of failure parameters in FDEM

3.2.1 Stiffness coefficient

The homogenization theory requires that the yield point and failure point of the joint element and the equivalent rock mass element remain consistent. When the joint element reaches its yield point and failure point, the rock mass element also reaches its yield limit and failure limit simultaneously. Figure 6 shows the stress–strain curves for rock, joints, and rock mass elements, which adopt elastic, elastoplastic and ideal elastoplastic constitutive models, respectively. According to the research of Abler et al.[26], the limit elastic strain $\varepsilon_a^{\mathrm{m}}$ and γ_a^{m}, limit plastic strain $\varepsilon_b^{\mathrm{m}}$ and γ_b^{m}, and strength at both the yield f_t and failure points f_s, can be determined for the rock mass element. By substituting the limit strain of the rock mass element at the yield point and failure point into the stress equilibrium equation (Eq.(6)) and the strain compatibility equation (Eq.(7)), the limit strain of the joint element at the yield point and failure point can be obtained:

$$\varepsilon_a^{\mathrm{j}} = \frac{h(E^{\mathrm{r}} - E^{\mathrm{m}})}{E^{\mathrm{r}}} \cdot \varepsilon_a^{\mathrm{m}} \tag{8}$$

$$\gamma_a^{\mathrm{j}} = \frac{h(G^{\mathrm{r}} - G^{\mathrm{m}})}{G^{\mathrm{r}}} \cdot \gamma_a^{\mathrm{m}} \tag{9}$$

$$\varepsilon_b^{\mathrm{j}} = h(\varepsilon_b^{\mathrm{m}} - \varepsilon_a^{\mathrm{m}}) + \varepsilon_a^{\mathrm{j}} \tag{10}$$

$$\gamma_b^{\mathrm{j}} = h(\gamma_b^{\mathrm{m}} - \gamma_a^{\mathrm{m}}) + \gamma_a^{\mathrm{j}} \tag{11}$$

where E^{m} represents the elastic modulus of engineering rock masses, which is determined based on the rock mass quality rating standard RQD. E^{r} is the elastic modulus of intact rock, which is obtained

through uniaxial compression tests. G^{m} and G^{r} denote the shear moduli of engineering rock masses and intact rock, respectively, which can be calculated using $G = E / (1+\nu)$, where E and ν denote the elastic modulus and Poisson's ratio of the rock material, respectively.

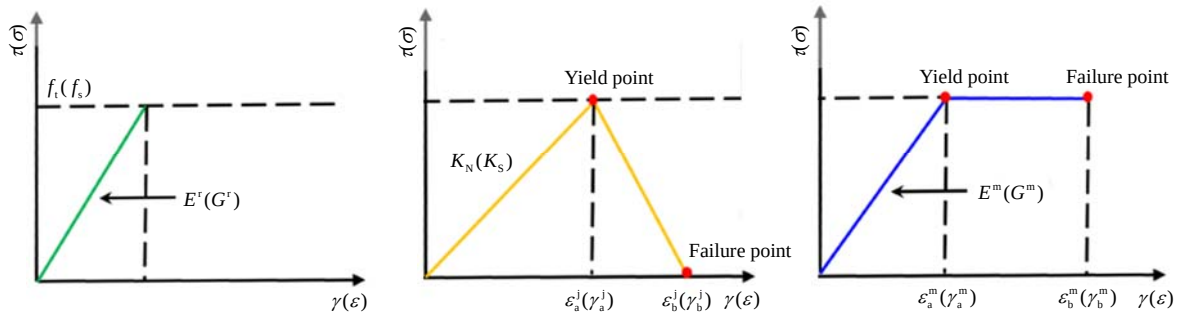

(a) Rock elements-linear elasticity (b) Joint elements-elastoplasticity (c) Rock mass unit-ideal elastoplasticity

Fig. 6 Constitutive relationships of rock, joint, and rock mass

3.2.2 Penalty parameters

The stress–strain relationship of the joint element during the linear elastic stage can be expressed as a stiffness matrix $[K^{\mathrm{e}}]$.

$$\mathrm{d}\boldsymbol{\sigma}^{\mathrm{j}} = [K^{\mathrm{e}}] = \begin{bmatrix} K_{\mathrm{N}} & 0 \\ 0 & K_{\mathrm{S}} \end{bmatrix} \mathrm{d}\boldsymbol{g} \tag{12}$$

where K_{N} and K_{S} represent the normal and tangential stiffness coefficients of the joint element in the linear elastic stage, respectively. According to Hooke's law, by combining Eqs.(8) and (9), we can obtain:

$$K_{\mathrm{N}} = \frac{f_{\mathrm{t}}}{\varepsilon_{\mathrm{a}}^{\mathrm{j}}} = \frac{E^{\mathrm{r}}E^{\mathrm{m}}}{h(E^{\mathrm{r}} - E^{\mathrm{m}})}, \quad K_{\mathrm{S}} = \frac{f_{\mathrm{s}}}{\gamma_{\mathrm{a}}^{\mathrm{j}}} = \frac{G^{\mathrm{r}}G^{\mathrm{m}}}{h(G^{\mathrm{r}} - G^{\mathrm{m}})} \tag{13}$$

The slope of the stress–displacement curve of the FDEM joint element in the pre-peak stage is the pre-peak stiffness coefficient of the joint element in the equivalent continuous model of the rock mass. Therefore, by combining Eqs.(2), (3) and (13), the formula for solving the penalty parameters of the joint element can be obtained.

$$p_{\mathrm{fn}} = \frac{E^{\mathrm{r}}E^{\mathrm{m}}}{(E^{\mathrm{r}} - E^{\mathrm{m}})} \tag{14}$$

$$p_{\mathrm{fs}} = \frac{G^{\mathrm{r}}G^{\mathrm{m}}}{(G^{\mathrm{r}} - G^{\mathrm{m}})} \tag{15}$$

Eqs.(14) and (15) give the relationship between the basic mechanical parameters of rocks and rock masses and the penalty parameters of joint elements in the FDEM algorithm.

3.2.3 Fracture energy

After yielding, the strain-softening stage of the FDEM joint element can be approximated using linear fitting[30]. The slope is different from that before yielding, and the area enclosed by the curve in the post-yield stage represents the fracture energy of the element. Therefore, the shear fracture energy G_{II} of the joint element can be derived as follows:

$$G_{\mathrm{II}} = f_{\mathrm{s}} \frac{\Delta\gamma^{\mathrm{j}}}{2} = f_{\mathrm{s}} \frac{\gamma_{\mathrm{b}}^{\mathrm{j}} - \gamma_{\mathrm{a}}^{\mathrm{j}}}{2} \tag{16}$$

where $\Delta\gamma^{\mathrm{j}}$ is the displacement change of the joint element in the post-yield stage. Combining Eqs.(9), (11) and (16), the following Eq. (17) can be obtained:

$$G_{\mathrm{II}} = \frac{hc^{\mathrm{m}}\cos\varphi^{\mathrm{m}}}{2\sqrt{3}(1-\sin\varphi^{\mathrm{m}})}\left(\gamma_{\mathrm{b}}^{\mathrm{m}} - \frac{2c^{\mathrm{m}}(1+\gamma^{\mathrm{m}})\cos\varphi^{\mathrm{m}}}{\sqrt{3}E^{\mathrm{m}}(1-\sin\varphi^{\mathrm{m}})}\right) \tag{17}$$

where c^{m} and φ^{m} represent the cohesion and internal friction angle of the equivalent rock mass element, respectively.

Eq.(17) provides the relationship between rock mass mechanical parameters and the fracture energy of joint elements in the FDEM algorithm.

3.3 Surrounding rock mass failure parameters

Based on the relationship the between mechanical parameters of rock or rock masses and the fracture algorithm parameters of surrounding rock masses derived in Section 3.2, the range of characteristic parameter values in FDEM can be calculated for different classes of surrounding rock masses. A railway tunnels is presented as an example, the mechanical parameter values for each class of surrounding rock masses are listed in Table 1[31]. Taking the intact rock blocks of coarse-grained diorite as an example, the penalty parameters and fracture energy for joint elements can be calculated, as listed in Table 2.

Table 1 Mechanical parameters of surrounding rocks and intact rock blocks with different classes

Surrounding rock mass class	Intact rock blocks		Engineering rock masses			
	Elastic modulus E^{r} /GPa	Poisson's ratio γ^{r}	Elastic modulus E^{m} /GPa	Poisson's ratio γ^{m}	Cohesion c^{m} /MPa	Internal friction angle φ^{m} /(°)
II	50	0.28	20～30	0.2～0.25	1.5～2.1	50～60
III	50	0.28	6～20	0.25～0.3	0.7～1.5	39～50
IV	50	0.28	1.3～6	0.3～0.35	0.2～0.7	27～39
V	50	0.28	<1.3	0.35～0.45	<0.2	20～27

Note: The data of intact rock blocks are from laboratory test results of coarse-grained diorite samples.

Table 2 Mechanical parameters of joint elements in surrounding rocks with different classes

Surrounding rock mass class	Normal stiffness /GPa	Tangential stiffness /GPa	Penalty parameters /(GPa • h)		Shear strain limit /‰		Shear fracture energy G /(J • m^{-2})
			p_{fn}	p_{fs}	γ_a^j	γ_b^j	
II	333–750	133.0–333.0	33.0–75.0	13.30–33.30	0.30–0.36	0.43–0.52	15.0–26.0
III	68–333	26.0–133.0	6.8–33.3	2.60–13.30	0.36–0.37	0.52–0.54	7.0–15.0
IV	13–68	4.9–26.0	1.3–6.8	0.49–2.60	0.37–0.39	0.54–0.57	1.7–7.0
V	2–13	4.5–4.9	0.2–1.3	0.45–0.49	0.36–0.39	0.50–0.65	1.3–1.7

Note: The grid size is chosen as 0.1 m.

4 Comparative analysis of simulating tunnel excavation process using FLAC^{3D} and FDEM

The finite difference method FLAC^{3D} and FDEM were adopted to simulate the tunnel excavation process under different rock mass classes and different cross-sections. The geometric dimensions of the models and the mechanical parameters of the surrounding rocks were the same in both methods. The tunnel sections were the double-line tunnel section for high-speed railways with a speed of 350 km/h and the single-line tunnel section for mixed passenger and freight railways with a speed of 160 km/h [2]. The classes III and IV surrounding rock mechanical parameters were determined based on the *Specifications for design of highway tunnels (section 1)* (JTG 3370.1−2018) [31], and are taken as the 1/2 quantile value. According to Tables 1 and 2, the calculation parameters are finally determined, as listed in Tables 3 and 4. For FDEM, the calculation grid uses a uniform grid with an element length of 0.1 m, while the FLAC^{3D} model uses the Mohr-Coulomb constitutive model. The simulation results using these two methods are shown in Figs.7–10. From Figs.7–10, it can be observed that the simulation results of tunnel excavation using FLAC^{3D} and FDEM are basically consistent under the same condition. The distribution of the plastic zone and the crack zone calculated using both methods matches well, which primarily locate at the spandrel, sidewall, and arch feet, and the overall distribution range is arc-shaped, with the widest distribution at the sidewall. For the class IV surrounding rock masses, the depths of the plastic zone and crack zone almost equal the tunnel diameter, and there are also a small number of distributions at the arch crown and inverted arch, as shown in Figs. 7(a), 7(c), 8(a), and 8(c). As the rock mass strength increases to class III, the distribution range of the plastic zone and crack zone sharply decreases, only distributed in the shallow part of the excavation section, while the rock mass at the arch crown and inverted arch positions remains intact, as shown in Figs. 9(a), 9(b), 10(a), and 10(b). Comparing the rock mass failure zones calculated by the two methods, it can be found that for class IV surrounding rock masses, the size and distribution of the failure zone of two tunnels after excavation are basically similar, both are distributed at the spandrel, sidewall, and arch feet, presenting a V-shaped pattern, as illustrated in Figs. 7(b) and 7(d). Furthermore, with increasing the height-span ratio of the tunnel section, the V-shaped opening of the failure zone becomes larger, as presented in Figs. 8(b) and 8(d), and the worst damage occurs at the sidewall for all tunnels. For class III surrounding rock masses, although plastic zones or crack zones are produced for two tunnels, rock masses exhibits small deformation. FLAC^{3D} results indicate that no failure zone is produced for class III surrounding rock masses. Also one can see from Figs. 9(c) and 10(c) that the tunnel remains stable when using FDEM. Finally, the simulation results using these two methods show that they also have similarities in the failure pattern of rock masses, mainly characterized by shear failure, with slight tensile failure in the shallow part of the excavation section.

Due to the differences in failure parameters and failure criteria between the two methods, there are also differences in the simulation results. For example, the FDEM simulation results show that the depth of the failure zone is slightly smaller than that of FLAC^{3D} results, as shown in Figs. 7(b), 7(d), 8(b), and 8(d). This can be attributed to the fact that in the continuum model, rock masses retain its continuous properties after failure, which is conducive to the transfer of stress between rock blocks, thereby promoting the expansion of the failure zone. In contrast, FDEM is able to better simulate the loosening, spalling, and

Table 3 Mechanical parameters of surrounding rocks and intact rock blocks with different classes used in two methods

Surrounding rock mass class	Intact rock blocks		Engineering rock masses			
	Elastic modulus E^r /GPa	Poisson's ratio γ^r	Elastic modulus E^m /GPa	Poisson's ratio γ^m	Cohesion c^m /MPa	Internal friction angle φ^m /(°)
III	50	0.28	13.00	0.275	1.10	44.5
IV	50	0.28	3.65	0.325	0.45	33.0

Table 4 Mechanical parameters of joint elements in surrounding rocks with different classes used in two methods

Surrounding rock mass class	Stiffness /GPa		Penalty parameters /(GPa • h)		Shear strain limit /‰		Shear fracture energy G /(J • m^{-2})
	K_N	K_S	p_{fn}	p_{fs}	γ_a^j	γ_b^j	
III	200.5	79.50	20.05	7.950	0.365	0.530	11.00
IV	40.5	15.45	4.05	1.545	0.380	0.555	4.35

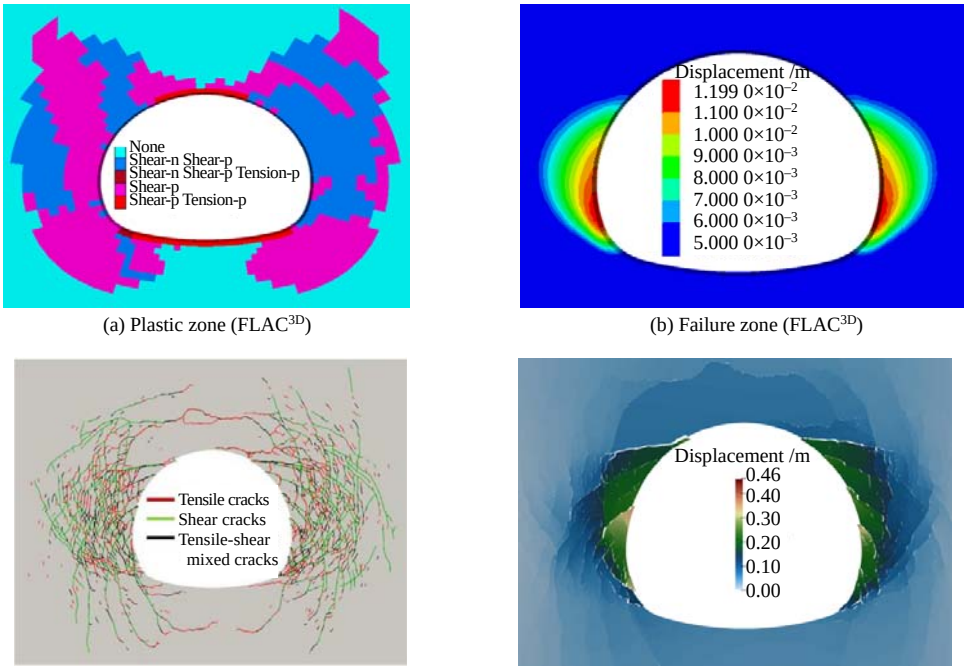

(a) Plastic zone (FLAC^{3D}) (b) Failure zone (FLAC^{3D})

(c) Crack zone (FDEM) (d) Failure zone (FDEM)

Fig. 7 Simulation results of excavation of the tunnel at a speed of 350 km/h in Class IV surrounding rocks

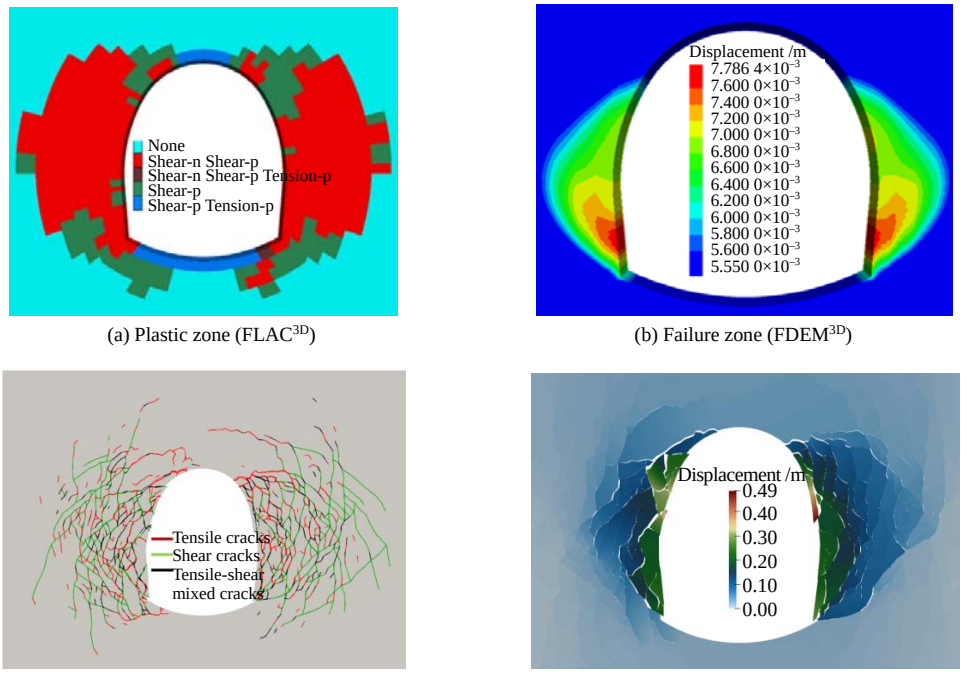

(a) Plastic zone (FLAC^{3D}) (b) Failure zone (FDEM^{3D})

(c) Crack zone (FDEM) (d) Failure zone (FDEM)

Fig. 8 Simulation results of excavation of the tunnel at a speed of 160 km/h in Class IV surrounding rocks

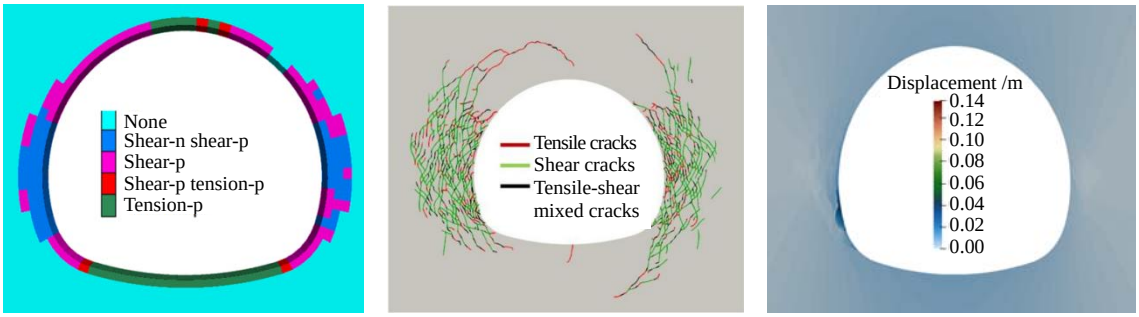

(a) Plastic zone (FLAC^{3D}) (b) Crack zone (FDEM) (c) Failure zone (FDEM)

Fig. 9 Simulation results of excavation of the tunnel at a speed of 350 km/h in Class III surrounding rocks

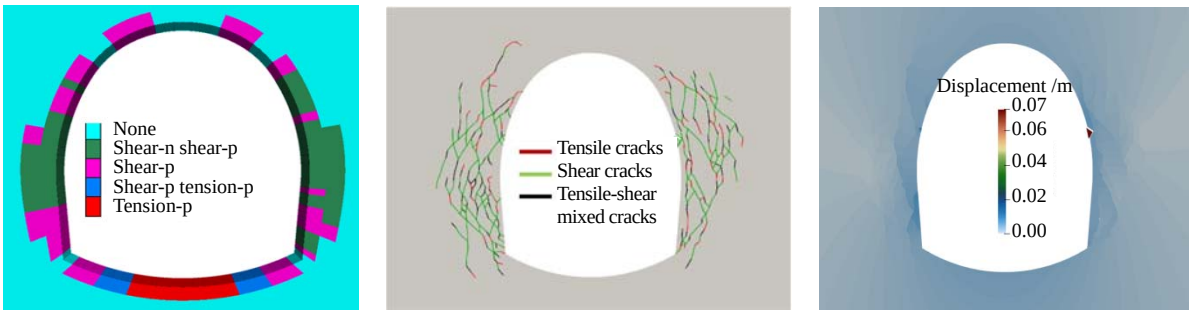

(a) Plastic zone (FLAC^{3D}) (b) Crack zone (FDEM) (c) Failure zone (FDEM)

Fig. 10 Simulation results of excavation of the tunnel at a speed of 160 km/h in Class III surrounding rocks

collapsing processes of surrounding rock masses after excavation disturbance, which is more in line with actual engineering conditions. It should also be noted that in FDEM, cracks are generated in both the arch crown and inverted arch after tunnel excavation. Regarding class IV surrounding rock masses, penetrating cracks are even produced at the arch crown, as presented in Figs. 7(c) and 8(c). However, in FLAC^{3D}, there is only a very small range of plastic zones in the arch crown and inverted arch (Figs. 7(a) and 8(a)), which is obviously inconsistent with the actual situation. Therefore, compared to FLAC^{3D}, the simulation results using the FDEM method can better ensure the safety of the arch crown and inverted arch of tunnels. Finally, the failure modes using the two methods are mainly characterized by shear failure, with a small amount of tensile failure zones in the shallow part of the tunnel section. However, in the FDEM model, the distribution range of tensile cracks is wider, mainly concentrated at the two sidewalls, as shown in Figs. 7(c) and 8(c). In FLAC^{3D} model, on the other hand, there is only a small amount of tensile failure zones distributed at the crown and invert arch positions of the tunnel (Figs. 7(a) and 8(a)). Therefore, the FDEM simulation results can more accurately reflect the characteristic that the tensile strength of geomaterials is much lower than the shear strength.

In summary, FLAC^{3D} and FDEM exhibit similar behaviors in simulating tunnel excavation, such as the expansion of the plastic zone or crack zone, the distribution range of the failure zone, and the failure mode of surrounding rock masses. Additionally, FDEM is capable of better simulating the progressive transition of surrounding rock masses from a continuous state to a discontinuous state under the effect of excavation unloading.

5 Conclusions

Two methods are selected in this paper, including the continuous medium analysis method and the continuous-discontinuous method represented by FDEM. Based on the basic theory and constitutive models of these two methods, this paper focuses on the identification of failure criteria for rock masses. A theoretical connection between the parameter values of these two methods is established for the first time, and a method for the rational and rapid determination of rock mass failure parameters is proposed in FDEM. Based on this, a comparative analysis is conducted on the simulated failure zones of surrounding rock masses of railway tunnels with different lithology and cross-sections during excavation. The following conclusions are drawn:

(1) The plastic strain limit is the criterion for surrounding rock mass failure in the continuous medium method, while the criterion is joint element opening or shear failure in FDEM.

(2) The relationship between the mechanical parameters of interface elements and the mechanical parameters of rock and rock mass elements are derived. The relationship between the mechanical parameters of rock masses and the parameters for rock mass failure algorithm is also established. The ranges for the main parameters of rock mass failure, such as penalty parameters and fracture energy in different classes of surrounding rock masses in FDEM (continuous-discontinuous methods), was provided. This solves the problem of the difficulty in rapidly obtaining reasonable values for rock mass failure parameters in continuous-discontinuous methods.

(3) The FLAC^{3D} and FDEM models were used to simulate the excavation process of railway tunnels with different lithology and cross-sections. The results demonstrate that the expansion patterns of the plastic zone or crack zone, the distribution range of the failure zone, and the failure pattern of surrounding rocks are generally consistent between the two methods. This indicates that the proposed method for determining the parameters of surrounding rock mass failure in FDEM is reasonable and feasible.

References

[1] ZHANG Ding-li, TAI Qi-min, FANG Qian. Safety of complex surrounding rock of tunnels and related evaluation method[J]. Chinese Journal of Rock Mechanics and Engineering, 2017, 36(2): 270–296.

[2] XIAO Ming-qing. Total safety factor method of tunnel support structure design[M]. Beijing: China Communication Press, 2020.

[3] LIU Xue-zeng, LIU Wen-yi, SUO Chao-feng. Effects of

the joint dip angle on the collapsed arch of surrounding rock around a highway tunnel[J]. Modern Tunnelling Technology, 2014, 51(6): 73–77.

[4] LI Zhan-jin, XU Dong-qiang. The research and development of theory of timbering soft rock laneway and mechanism[J]. Journal of Hebei Institute of Technology, 2003(4): 8–13.

[5] WANG Rui, ZHANG Yu, HUANG Xiao-dong, et al. Optimization of bolt support for soft rock large deformation tunnel based on the theory of loose circle[J/OL]. Journal of Civil and Environmental Engineering, 1-8. http://kns.cnki.net/kcms/detail/50.1218.TU.20211004.1841.002.html.

[6] HAN Xing-bo, YE Fei, FENG Hao-lan, et al. Pressure of surrounding rock of deep-buried loess shield tunnel[J]. Chinese Journal of Geotechnical Engineering, 2021, 43(7): 1271–1278, 1377.

[7] LI Yong-an, GUO Xiao-fei, MA Nian-jie, et al. Research status and evaluation of theoretical calculation of plastic zone boundary for hole surrounding rock[J]. Coal Science and Technology, 2021, 49(5): 141–150.

[8] HUANG Long-xian, YANG Tian-hong, ZHENG Chao, et al. Influence of anisotropy on failure mode of tunnel under different lateral pressures[J]. Journal of Northeastern University (Natural Science), 2012, 33(5): 739–742.

[9] HU Gao-jian, YANG Tian-hong, ZHANG Fei, et al. Parallel computing technologies for the failure mode and area of surrounding rock in complex goafs[J]. Journal of Mining & Safety Engineering, 2017, 34(3): 565–572.

[10] WU Cheng, ZHANG Ping. Analysis of numerical simulation methods for excavation failure zone of deep underground opening in hard rocks with high geostress[J]. Hydrogeology & Engineering Geology, 2012, 39(6): 35–42.

[11] CHEN Deng-hong, HUA Xin-zhu, DUAN Ya-wei, et al. Simulation of zonal tensile and compressive deformation and failure of surrounding rock in deep large deformation mining gateway[J]. Rock and Soil Mechanics, 2016, 37(9): 2654–2662.

[12] LIU Xue-sheng, FAN De-yuan, TAN Yun-liang, et al. Failure and instability mechanism of anchored surrounding rock for deep chamber group with super-large section under dynamic disturbances[J]. Rock and Soil Mechanics, 2021, 42(12): 3407–3418.

[13] YUAN Yue, WANG Wei-jun, YUAN Chao, et al. Large deformation failure mechanism of surrounding rock for gateroad under dynamic pressure in deep coal mine[J]. Journal of China Coal Society, 2016, 41(12): 2940–2950.

[14] LI Ying, ZHANG Chang-suo, ZHENG Chen, et al. Analysis of numerical simulation methods for excavation damage zone of deep tunnels in hard rocks[J]. Journal of Taiyuan University of Technology, 2017, 48(5): 753–757.

[15] LEI Jiang, CHEN Wei-zhong, LI Fan-fan, et al. Mechanical properties of surrounding rock in diversion tunnel of water diversion project from Hongyan River to Shitou River[J]. Rock and Soil Mechanics, 2019, 40(9): 3435–3446.

[16] ZHENG Ying-ren, ZHU He-hua, FANG Zheng-chang, et al. The stability analysis and design theory of surrounding rock of underground engineering[M]. Beijing: China Communication Press, 2012.

[17] GAO Fu-qiang. Use of numerical modeling for analyzing rock mechanic problems in underground coal mine practices[J]. Journal of Mining and Strata Control Engineering, 2019, 1(1): 13004.

[18] LI Fan, ZHANG Qiang-yong, XIANG Wen, et al. Experimental, theoretical and computational analysis on the mechanism of splitting failure of high sidewall cavern[J]. Chinese Journal of Rock Mechanics and Engineering, 2023, 42(7): 1662–1679.

[19] WANG Xue-bin, DU Ya-zhi, PAN Yi-shan, et al. An elastic and brittle model with damage and application in study on rock localized failures[J]. Journal of Basic Science and Engineering, 2012, 20(4): 642–653.

[20] MA Bing, WANG Xue-bin, TIAN Feng. Comparative analysis of brittle failure characteristics of surrounding rock based on two numerical simulation methods[J]. Rock and Soil Mechanics, 2021, 42(12): 3440–3450.

[21] LI Dong-dong, SHENG Qian, XIAO Ming, et al. Meso-mechanism of surrounding rock local damage of underground powerhouse cavern based on improved particle flow acoustic emission sheet[J]. Rock and Soil Mechanics, 2022, 43(Suppl.2): 117–129.

[22] DENG Peng-hai, LIU Quan-sheng, HUANG Xing. FDEM numerical study on the fracture and swelling deformation of heterogeneous rock mass around tunnel based on Weibull distribution[J]. Engineering Mechanics, 2023: 1-24. http://kns.cnki.net/kcms/detail/11.2595.O3. 20230303. 1338.014.html.

[23] DENG P H, LIU Q S, LU H F. A novel joint element parameter calibration procedure for the combined finite-discrete element method[J]. Engineering Fracture Mechanics, 2022, 276: 108924.

[24] CHENG Shu-fan, GAO Rui, ZENG Ya-wu, et al. FDEM simulation of dynamic failure mechanism of coal rock under impact[J]. Journal of Vibration and Shock, 2022, 41(19): 136–143.

[25] ZHANG Shi-rui, QIU Shi-li, LI Shao-jun, et al. Study on mechanical properties of Beishan granite meso-heterogeneity under uniaxial compression with FDEM[J]. Chinese Journal of Rock Mechanics and Engineering, 2022, 41(Suppl.1): 2658–2672.

[26] ABI Er-di, FENG Xia-ting, ZHENG Ying-ren, et al. Strain analysis and numerical analysis based on limit strain for geomaterials[J]. Chinese Journal of Rock Mechanics and Engineering, 2015, 34(8): 1552–1560.

[27] DENG P H, LIU Q S, HUANG X, et al. Sensitivity analysis of fracture energies for the combined finite-discrete element method (FDEM)[J]. Engineering Fracture Mechanics, 2021, 251: 107793.

[28] YAN C Z, JIAO Y Y. A 2D fully coupled hydro-mechanical finite-discrete element model with real pore seepage for simulating the deformation and fracture of porous medium driven by fluid[J]. Computers & Structures, 2018, 196: 311–326.

[29] LIU Xin-rong, HAN Ya-feng, ZHOU Xiao-han, et al. Model test on the progressive failure characteristics of tunnel-type anchorage in soft rock[J]. Chinese Journal of Rock Mechanics and Engineering, 2022, 41(9): 1760–1770.

[30] PROFIT M, DUTKO M, YU J G, et al. Complementary hydro-mechanical coupled finite/discrete element and microseismic modelling to predict hydraulic fracture propagation in tight shale reservoirs[J]. Computational Particle Mechanics, 2016, 3(2): 229–248.

[31] China Merchants Chongqing Communications Technology Research & Design Institute Co., LTD. JTG 3370.1—2018 Specifications for design of highway tunnels (section 1): civil engineering[S]. Beijing: China Communications Press, 2019.